Evaluation of the Hydrodynamic Properties and Performance Efficiency of a Three-Row Permeable Vertical Breakwater

Tarek A. Eldamaty
Civil Engineering Department, Umm Al-Qura University, College of Engineering and Architecture, Saudi Arabia
tadamaty@uqu.edu.sa

Medhat M. Helal
Civil Engineering Department, Umm Al-Qura University, College of Engineering and Architecture, Saudi Arabia
mmhelal@uqu.edu.sa (corresponding author)

Received: 27 February 2024 | Revised: 17 March 2024 | Accepted: 26 March 2024

 DOI: https://doi.org/10.48084/etasr.7152

ABSTRACT

Coastal protection structures reduce risks and economic losses by eliminating coastal erosion, wave damage, and flooding. Fixed breakwaters are used along the coast but are often inappropriate due to their negative environmental impact. Permeable breakwaters resemble a row of breakwaters with continuous walls and are proposed as a more environmentally friendly alternative. The wave-structure interaction and flow behavior of this type of breakwater are more complex but must be analyzed before designing it. This study develops a mathematical model of wave interaction with a permeable three-row vertical breakwater based on the least squares method. Comparison with experimental measurements of the reflection, transmission, and dissipation coefficients shows that the mathematical model adequately reproduces most of the important features of the results. This study provides a deeper understanding of the hydrodynamic performance of a permeable three-row vertical continuous wall breakwater.

Keywords-permeable barriers; slotted breakwaters; mathematical concepts; coefficient of transmission; coefficient of reflection; coefficient of dissipation of energy

I. INTRODUCTION

The development of coastal areas has a significant impact on the national revenues of numerous countries around the world. Preserving the coastal area, harbors, and marine life by employing the best techniques that are least expensive, environmentally benign, and have the least negative effects on the adjoining coasts are among the main concerns related to these areas. Artificial beaches, breakwaters, jetties, seawalls, artificial headlands, and groins are just a few examples of coastal protection systems. Breakwaters are often placed near beaches, harbors, marinas, shorelines, and channel entrances to protect the shore by reducing the wave height and the current velocity that can be carried down the coast and within harbors. Breakwaters are divided into two categories based on the level of protection they provide. In partial or non-conventional protection, breakwaters have been more recently employed and have proven to overcome the limitations of conventional breakwaters. Full protection or conventional breakwaters are widely implemented but have inherent drawbacks, such as being massive, harmful to the environment, causing excessive reflections, and not being cost-effective in deeper waters [1].

Several breakwater varieties provide partial protection, including submerged, floating, flexible, detachable, perforated, pile, pipe, and slotted models [2]. Pneumatic and hydraulic breakwaters are also available. The flow behavior across slotted breakwaters is complex, and more research is needed to understand their hydrodynamic properties and wave-responsive performance efficiency. The phenomena become more complex when a multi-row array of slotted walls is used. Due to the complexity of the wave interaction with these structures, studies have focused on theoretical and experimental investigations to comprehend flow behavior through a collection of slotted walls [3]. Numerous investigations have been conducted to suggest slotted breakwater layouts, improve their functionality, and examine their hydrodynamic behavior in terms of attenuating incident waves. In particular, the development of various geometric configurations has received a great deal of attention. Deploying numerical models, several attempts have also been made to comprehend the physical behavior of the breakwater's activity.

In [4], the wave transmission coefficient (C_T) and the acting wave forces (F) for a vertical slotted breakwater were

theoretically and experimentally examined. This study proposed a straightforward method for calculating C_T and F, which is mainly based on the losses caused by the slot gap. In [5-6], a numerical computation established on Stokes's first-order theory was presented following an eigenfunction expansion approach for wave interaction with a single and paired thin vertical slotted barrier that spans from the water surface to a certain distance above the seabed. The results exhibited good agreement with the experimental measurements of the transmission, reflection, and dissipation coefficients, suggesting that the energy dissipation by the barrier is effectively calculated by the numerical method. In [7], the relationship between waves and slotted breakwaters was investigated deploying an eigenfunction expansion and linear wave theory. This study revealed that the porosity of the slotted plate, which is the fundamental variable that defines the structure permeability, and the height of the incident waves are the main factors that influence the reflection characteristics of a slotted sea wall. In [8], analytical models predicated on potential flow were developed to predict wave reflection from a perforated wall caisson breakwater. Additionally, studies of irregular waves with different significant wave heights and chamber widths were experimentally carried out. The reflected wave spectrum was found to have frequency-dependent oscillating behavior. This model was modified for the current work.

In [9], horizontal slotted wave screens with circular intercepting elements were explored by contrasting the numerical model derived from Green's identity formula with the experimental findings. In [10-11], the hydrodynamic properties of pile-supported vertical wall breakwaters with square and circular piles under regular and irregular waves were explored. Analysis and estimation of the reflection, transmission, run-up, and wave forces acting on the breakwater were carried out adopting the eigenfunction expansion approach. This technique was also expanded to include random waves. In [12], an experimental and theoretical study was performed on a single row of vertically slotted breakwaters under normal, regular waves. This study proposed a straightforward theoretical framework utilizing an eigenfunction, which was evaluated by contrasting the theoretical model's output with theoretical and experimental findings from various investigations. The results indicated that the transmission coefficient drops when dimensionless wave number increases, wave steepness increases, and breakwater porosity decreases. It was concluded that, by adopting the friction coefficient f = 1.5, the theoretical model could be implemented to estimate both the performance of slotted breakwaters and the hydrodynamic forces that act on these structures.

In [13], a numerical model was recommended based on an eigenfunction expansion method for normal linear wave interactions with a single or double vertical slotted wall and nonlinear (Stokes second-order) wave interactions with a single vertical slotted wall. Experimental results and comparisons with other studies validated the proposed numerical model. This study also demonstrated that reflection (C_R), transmission (C_T), and energy losses (C_E) of permeable breakwaters are significantly influenced by f and the coefficient of porosity (ε), but that the added mass coefficient (C_m) has little effect and can be ignored for this configuration. In [14], the hydrodynamic performance of a wave-absorbing double curtain-wall breakwater was studied. A shoreward impermeable wall and a seaward perforated wall made up the breakwater. The wave forces acting on the walls and the reflection and transmission coefficients were computed. In [15], High-Performance Glass Fibre Reinforced Concrete (HPGFRC) was used to propose a new type of shell precast concrete block for coastal constructions. With stronger qualities including shrinkage, abrasion resistance, and waterproof grade, HPGFRC promised to shield the reinforcement from the harsh marine environment and corrosion, extending the structure's service life.

In [16], the hydrodynamic properties of three rows of vertical slotted breakwaters were reviewed. The third wall is impermeable, while the front and middle were permeable walls partially submerged in a water channel of constant depth. To investigate the hydrodynamic performance of a breakwater, a mathematical model based on the eigenfunction expansion approach and a least square technique was put into service for wave interaction. The transmission, reflection, energy dissipation, wave run-up, and wave force were theoretically explored under typical regular waves. This study provided a clearer understanding of the hydrodynamic performance of a triple-row vertical slotted wall breakwater. In [17], the wave transmission coefficient (C_T) was obtained for three different types of pile breakwaters in coastal areas. In [18], it was analyzed how floating, submerged, and piled breakwater performed differently depending on changes in key characteristics.

This study aims to characterize the hydraulic performance and flow characteristics of a permeable three-row vertical continuous wall breakwater with irregular geometries, extending [19-22]. A mathematical nonlinear model (Stokes second order) was drawn based on an eigenfunction expansion method and a least-squares technique.

II. MATHEMATICAL FORMULATION

Figure 1 depicts a triple-row vertical slotted wall breakwater, where b is the wall's thickness and d is the water depth. A Cartesian coordinate system (x and z) is defined as follows: the vertical coordinate (z) is measured vertically upward from the water line, and the positive x is directed from a point of the first wall to the left.

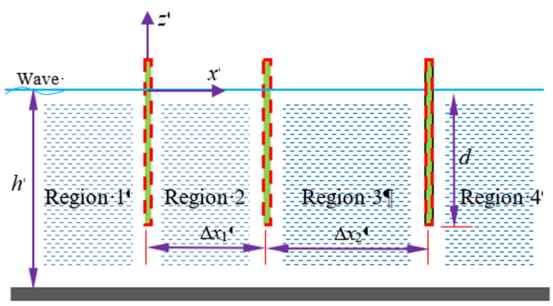

Fig. 1. Sectional view of the domains.

A free surface boundary in the water wave moves in tandem with the velocity of the water particles. The velocity is unknown. As a result, before computation, the location of the free surface border is uncertain. The three walls split the fluid domain into four areas. The Laplace equation is satisfied by the existence of the velocity potential, assuming an incompressible fluid and irrotational flow motion. The velocity potential $\Phi(x, z, t)$ in each region has the following boundary value for monochromatic incident waves with angular frequency ω at time t:

$$\Phi(x,z,t) = Re[\phi(x,z)e^{-i\omega t}] \quad (1)$$

where φ, and Re[] stand for the spatial velocity potential and the real component of the argument, respectively, and $i = \sqrt{-1}$. The velocity potential fulfills the Laplace equation under the assumptions of an incompressible fluid and irrotational flow motion. The spatial velocity in each region yields the following boundary value problem:

$$\frac{\partial^2\phi_j}{\partial x^2} + \frac{\partial^2\phi_j}{\partial z^2} = 0, \ j = 1,2,3,4 \quad (2)$$

where the variables in the area j are represented by the subscript j. Additionally, these potentials are needed to meet the proper boundary conditions on the free surface:

$$\frac{\partial\phi_j}{\partial z} - \frac{\omega^2}{g}\phi_j = 0, \text{ at } z = 0 \text{ and } j = 1,2,3,4 \quad (3)$$

$$\frac{\partial\phi_j}{\partial z} = 0, \text{at } z = -h, \quad j = 1,2,3,4 \quad (4)$$

$$\lim_{x\to-\infty}\left(\frac{\partial\phi_R}{\partial z} + ik_0\phi_R\right) = 0, \text{ and}$$

$$\lim_{x\to+\infty}\left(\frac{\partial\phi_4}{\partial z} - ik_0\phi_4\right) = 0 \quad (5)$$

where ϕ_R is the velocity potential of reflected waves, g is the gravitational acceleration, and k_0 is the incident wave number. Furthermore, the eigenfunction expansion approach used in [5, 10] provides the reduced velocity potentials ϕ. There is an endless number of ways to express the velocity potentials. The following are the solutions to (2) that meet the boundary conditions (3)-(5):

$$\phi_1 = -\frac{igH}{2\omega}\times$$
$$[e^{-\alpha_0 x}Z_0(z) + R_0 e^{\alpha_0 x}Z_0(z) + \sum_{n=1}^{\infty} R_n e^{\alpha_n x}Z_n(z)] \quad (6)$$

$$\phi_2 = -\frac{igH}{2\omega}\times$$
$$\left[\sum_{n=0}^{\infty} A_n e^{-\alpha_n x}Z_n(z) + \sum_{n=0}^{\infty} C_n e^{\alpha_n(x-a)}Z_n(z)\right] \quad (7)$$

$$\phi_3 = -\frac{igH}{2\omega}\times$$
$$\left[\sum_{n=0}^{\infty} B_n e^{-\alpha_n(x-a)}Z_n(z) + \sum_{n=0}^{\infty} D_n e^{\alpha_n(x-b)}Z_n(z)\right] \quad (8)$$

$$\phi_4 = -\frac{igH}{2\omega}\times$$
$$\left[T_0 e^{-\alpha_0(x-b)}Z_0(z) + \sum_{n=1}^{\infty} T_n e^{-\alpha_n(x-b)}Z_n(z)\right] \quad (9)$$

where the coefficients of the component waves moving forward and backward are, R_n, A_n, B_n, C_n, D_n and T_n (n = 0, 1, 2, …), respectively. The solutions to the first-order dispersion relation $\omega^2 = -gk_n\, tan(\, k_n h)$ [5, 23] are the wave numbers $\alpha_n = k_n, n = 1,2, \ldots$. Non-propagating evanescent waves have an infinite discrete set of real roots $\pm k_n$ for $(n \geq 1)$, while propagating waves have a pair of imaginary roots ($\alpha_0 = \pm ik_0$). The negative sign is utilized to correspond the propagating waves in (6)-(9) to the reflected and transmitted waves. For the non-propagating waves to disappear exponentially with increasing distance from the wall, the positive roots for $n \geq 1$ are taken. The depth-dependent functions $Z_n(z)$ (n = 0, 1, 2, …) in (6)-(9) are provided by:

$$Z_0(z) = \frac{cosh\, k_0(z+h)}{cosh(k_0 h)}, \quad Z_n(z) = \frac{cos\, k_n(z+h)}{cos(k_n h)} \quad (10)$$

The requirements that the horizontal velocities at the breakwater should be equal are automatically satisfied by (6)-(9), which also meet all other pertinent boundaries. As a result, at the breakwater interfaces, the velocity potentials must meet the following boundary conditions:

$$\frac{\partial\phi_1}{\partial x} = \frac{\partial\phi_2}{\partial x} = ik_0 G(\phi_1 - \phi_2), x = 0, -d \leq z \leq 0 \quad (11)$$

$$\frac{\partial\phi_1}{\partial x} = \frac{\partial\phi_2}{\partial x}, x = 0, -h \leq z \leq -d \quad (12)$$

$$\phi_1 = \phi_2, \ x = 0, \ -h \leq z \leq -d \quad (13)$$

$$\frac{\partial\phi_2}{\partial x} = \frac{\partial\phi_3}{\partial x} = ik_0 G(\phi_2 - \phi_3), \quad (14)$$
$$x = a, -d \leq z \leq 0$$

$$\frac{\partial\phi_2}{\partial x} = \frac{\partial\phi_3}{\partial x}, x = a, \quad -h \leq z \leq -d \quad (15)$$

$$\phi_2 = \phi_3, \ x = a, \quad -h \leq z \leq -d \quad (16)$$

$$\frac{\partial\phi_3}{\partial x} = \frac{\partial\phi_4}{\partial x} = ik_0 G(\phi_3 - \phi_4), \quad (17)$$
$$x = b, -d \leq z \leq 0$$

$$\frac{\partial\phi_3}{\partial x} = \frac{\partial\phi_4}{\partial x}, x = b, -h \leq z \leq -d \quad (18)$$

$$\phi_3 = \phi_4, x = b, -h \leq z \leq -d \quad (18)$$

Therefore, G can be expressed by:

$$G = \frac{\varepsilon}{b(f - is)} = |G|e^{i\theta}, 0 \leq \theta \leq \pi/2 \quad (20)$$

where G is the permeability parameter of a thin perforated wall, which is often complex, and θ is the argument of the complex G. The perforated wall becomes totally transparent when $|G|$ tends towards infinity, whereas it reduces to an impermeable wall when $|G|$ equals zero. The porosity of the wall's perforated area is denoted by ε, the friction coefficient is represented by f, and the wall thickness is denoted by b. The inertia coefficient denoted by s is provided by:

$$s = 1 + C_m\left(\frac{1-\varepsilon}{\varepsilon}\right) \quad (21)$$

where C_m denotes the increased mass coefficient and is handled as a constant. As recommended in [5], f = 2.0 and C_m are treated as constants (C_m=0). It is observed that both wave energy dissipation and wave motion phase shift can occur when waves go through a narrow-perforated wall. The real part of G is affected by the energy dissipation brought on by the wall's resistance effect. However, the imaginary part of G is influenced by the phase shift brought on by the wall's inertial

action. The perforated wall becomes impermeable when |*G*| equals zero, and completely transparent when |*G*| trends towards infinity.

III. EXPERIMENTAL SETUP AND MEASUREMENTS

The hydrodynamic performance of a wave absorber consisting of three rows of vertical slotted wall breakwaters was investigated through a series of experiments conducted in a wave flume. The wave flume was 15 m in length, 0.30 m in width, and 0.45 m in depth, as detected in Figures 2 and 3. At one end of the flume, a computer-controlled flap-style wave generator produces consistent waves of varying heights and frequencies, while at the other end, a porous beach serves as a wave absorber. The study was carried out using regular generator waves with varying wave periods (T = 0.5-2 s) and a constant water depth (h) of 25 cm. The curtain walls, the intervals between rows, and the porosities were all arranged differently in the tests. The first vertical wall was positioned at the center of the wave flume. The distance between the first and third walls remained constant at $x_3 - x_1 = 2h$, while the second wall's position was adjusted to produce Δx_1 values of 0.50, 1.50, and 2.0 m, respectively.

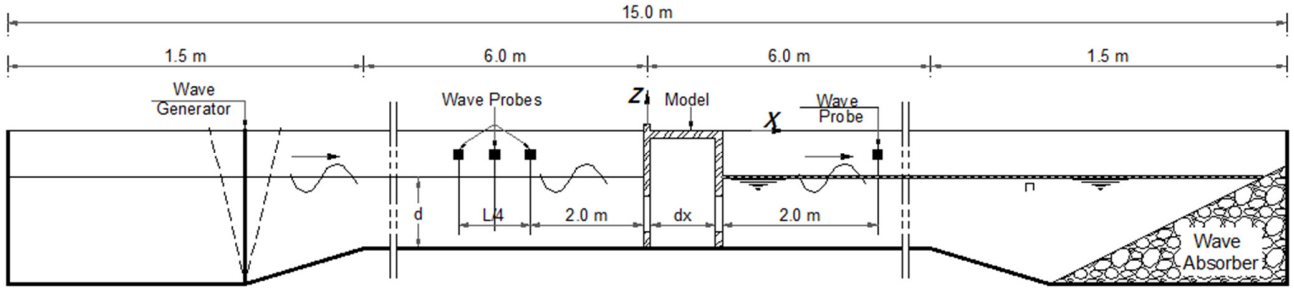

Fig. 2. Experimental setup.

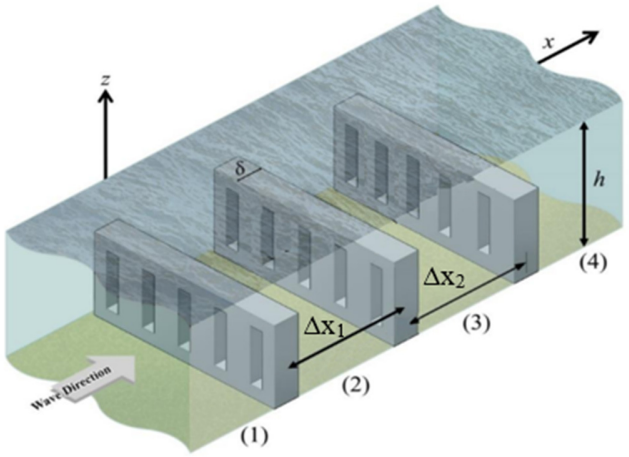

Fig. 3. Sectional elevation view of the domains for the breakwater.

The vertical panels that made up the suggested breakwater models had a width of 0.025 m and a thickness of the same amount. The porosity of the slotted walls was set at $\varepsilon = 0.5$. The models were made of aluminum. Four wave probes were employed to measure the water's surfaces. Three probes were placed in front of the model at a distance equal to the longest wavelength from the second wall that was tested. To compute the reflection coefficient following the three-probe approach of [24], the spacing between the first three probes was varied for each wave period. Three wave probes were deployed to minimize inaccuracies in phase and amplitude measurements. The wave probe was placed 2.0 m away from the model at its back and was utilized to measure the wave transmission.

TABLE I. ESTIMATION OF THE TRANSMISSION AND REFLECTION COEFFICIENTS

Frequency (Hz)	Water depth (m)	Wave height (m)	Reflection coefficients C_R	Transmission coefficients C_T
0.50	0.25	0.045	0.29	0.61
0.75	0.25	0.040	0.33	0.47
1.00	0.25	0.035	0.48	0.42
1.25	0.25	0.030	0.52	0.38
1.50	0.25	0.025	0.64	0.26
1.75	0.25	0.020	0.71	0.19
2.00	0.25	0.015	0.82	0.08

IV. THE MATHEMATICAL SOLUTION

The expressions for ϕ_j, where j = 1, 2, 3, 4, that meet the boundary criteria along $x = x_i$ and the conditions for convection, free surface, and seafloor in (11)-(19) are simplified to:

$$\frac{\partial \phi_1}{\partial x} = \frac{\partial \phi_2}{\partial x}, x = 0 \quad (22)$$

$$\frac{\partial \phi_1}{\partial x} = ik_0 G(\phi_1 - \phi_2), x = 0, -d \le z \le 0 \quad (23)$$

$$\phi_1 = \phi_2, x = 0, -h \le z \le -d \quad (24)$$

$$\frac{\partial \phi_2}{\partial x} = \frac{\partial \phi_3}{\partial x}, x = a \quad (25)$$

$$\frac{\partial \phi_2}{\partial x} = ik_0 G(\phi_2 - \phi_3), x = a, -d \le z \le 0 \quad (26)$$

$$\phi_2 = \phi_3, x = a, -h \le z \le -d \quad (27)$$

$$\frac{\partial \phi_3}{\partial x} = \frac{\partial \phi_4}{\partial x}, x = b \quad (28)$$

$$\frac{\partial \phi_3}{\partial x} = ik_0 G(\phi_3 - \phi_4), x = b, -d \le z \le 0 \quad (29)$$

$$\phi_3 = \phi_4, x = b, -h \le z \le -d \quad (30)$$

Replacing the velocity potential formulations from (6)-(9) into (22)-(30) and implementing the least squares method to solve them for the coefficient values produces:

$$R_0 = 1 - A_0 + C_0 e^{-\alpha_0 a} \quad (31)$$

$$R_n = -A_n + (C_n + D_n - T_n) e^{-\alpha_n a}, n = 1,2,\ldots \quad (32)$$

Many engineering wave qualities can be obtained if the wave potentials are computed. The ratio of the reflected wave height to the incident wave height is known as the real reflection coefficient C_R:

$$C_R = |R_0| \quad (33)$$

The actual coefficients of transmission (C_T) are defined as the ratio of the transmitted wave height to the incident wave height:

$$C_T = |T_0| \quad (34)$$

It is possible to compute the energy-loss coefficient C_L via

$$C_L = \sqrt{1 - C_R^2 - C_T^2} \quad (35)$$

The dynamic pressure along the structure can be integrated to determine the wave force acting on each wall. The horizontal wave force magnitude on the front wall's unit width, F_f, is expressed as:

$$F_f = i\rho\omega \int_{-d}^{0} (\phi_1 - \phi_2)|_{x=0} dz \quad (36)$$

$$= \frac{\rho g H}{2ik_0 G}\left[(R_0 + 1)\frac{\sinh(k_0 h) - \sinh k_0 (h-d)}{ik_0 \cosh(k_0 h)} + \sum_{n=1}^{\infty} R_n \frac{\sin(k_n h) - \sin k_n (h-d)}{ik_n \cos(k_n h)}\right] \quad (37)$$

The horizontal wave force's magnitude on the back wall's unit width F_r is expressed as:

$$F_r = i\rho\omega \int_{-d}^{0} (\phi_3 - \phi_4)|_{x=b} dz \quad (38)$$

$$= \frac{\rho g H}{2}\left[(1 - T_0)\frac{\sinh(k_0 h) - \sinh k_0 (h-d)}{k_0 \cosh(k_0 h)} + \sum_{n=1}^{\infty}(B_n + D_n - T_n)\frac{\sin(k_n h) - \sin k_n (h-d)}{k_n \cos(k_n h)}\right] \quad (39)$$

The dimensionless wave forces C_{Ff} and C_{Fr} on the front and rear walls are defined as

$$C_{Ff} = \frac{|F_f|}{\rho g H h}, \qquad C_{Fr} = \frac{|F_r|}{\rho g H h} \quad (40)$$

V. RESULTS AND DISCUSSION

The numerical results of the three-vertical-slotted-wall breakwater were calculated using MATLAB tools version R2021b and were contrasted with the experimental findings. In the experimental work, regular waves, a fixed depth of water (h), and a consistent porosity (ε) for the permeable portion were used. There are distinct gaps between the first and third walls where the second wall is situated.

The wave interactions on this breakwater design are dictated by their characteristics of reflection, transmission, and dissipation. The reflection coefficient is employed to quantify the energy of the waves that are reflected back from the first permeable wall. The ratio of the reflected wave height to the incident wave height is known as the reflection coefficient C_R. The entire reflection is represented by a C_R value of one, and the entire wave transmission or absorption is represented by a C_R value of zero. The transmission coefficient C_T is used to quantify the energy of the waves that pass through the breakwater. Energy dissipation through the permeable component is related to the difference in energy between the incident wave and the total energy of the reflected and transmitted waves. The energy dissipation coefficient C_L is described by (35). The transmission and reflection coefficients of a triple vertical slotted wall breakwater are plotted against h/L, ω^2/gh, dk_0, and B/L, respectively. Figures 4, 5, 6, and 7 depict the comparison of the reflection and transmission coefficients between the experimental data for k_0h = 1.5, d/h = 0.5, and |G| = Infinity with the results of the current approach. These figures reveal that there is a satisfactory agreement between the numerical and the experimental results.

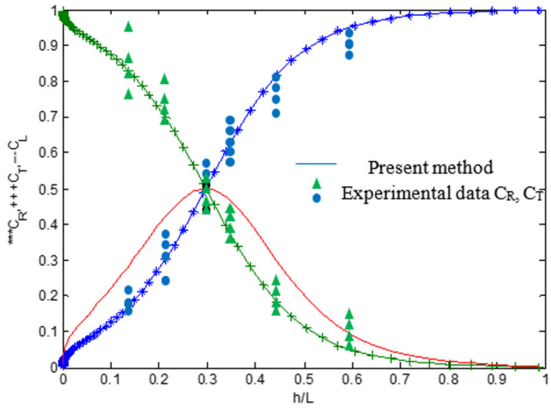

Fig. 4. Comparison between numerical and experimental results: C_R and C_T as a function of h/L for G=∞, k_0h=1.5, d/h=0.5, Δx_1=0.5d, and Δx_2 = 0.5d.

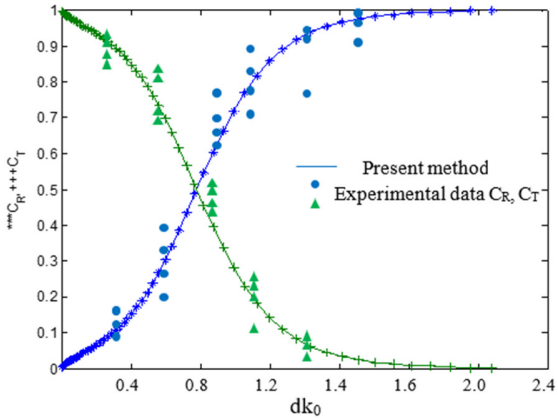

Fig. 5. Comparison between numerical and experimental results: C_R and C_T as a function of dk_0 for G=∞, k_0h=1.5, d/h=0.5, Δx_1=0.5d, and Δx_2=0.5d.

Figures 8 and 9 illustrate the effects of the breakwater's relative draft d/h on C_R and C_T at k_0h = 1.6, G = 0.5e^{0i}, Δx_1=0.5d, and Δx_2 = 0.5d as a function of the relative wave chamber width B/L. The reflection and transmission

coefficients in these figures are derived from the experimental data and the proposed method. Overall, the record of the experimental data may be satisfactorily reproduced by the numerical solution. For fixed *B/L*, the reflection coefficient C_R increases with *d/h*.

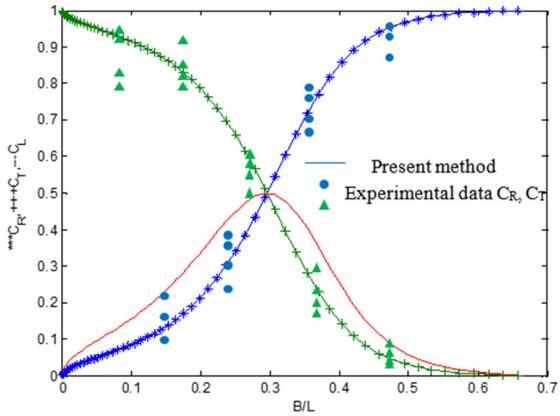

Fig. 6. Comparison between numerical and experimental results: C_R and C_T as a function of *B/L* for $G=\infty$, k_0h=1.5, *d/h*=0.5, Δx_1=0.5d, and Δx_2=0.5d.

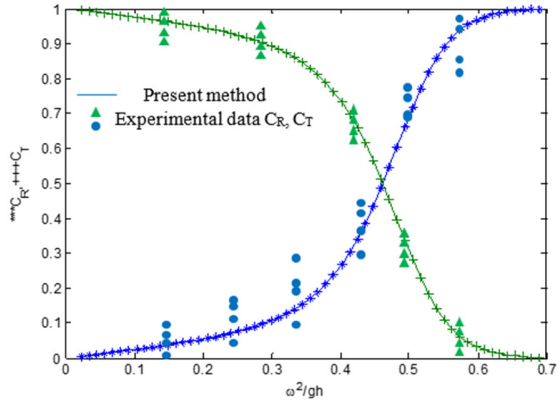

Fig. 7. Comparison between numerical and experimental results: C_R and C_T as a function of ω^2/gh for $G=\infty$, k_0h=1.5, *d/h*=0.5, Δx_1=0.5d, and Δx_2=0.5d.

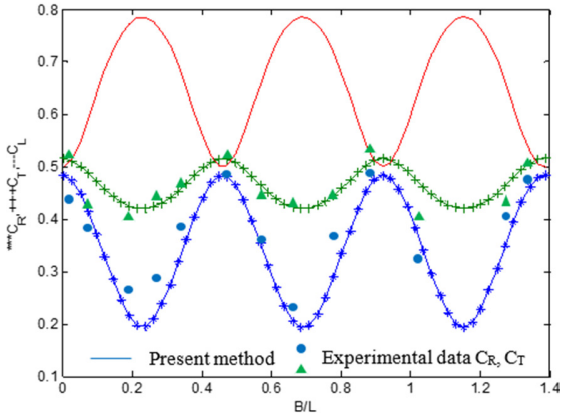

Fig. 8. Comparison between numerical and experimental results: C_R and C_T as a function of *B/L* for k_0h=1.6, G=0.5e^{0i}, Δx_1=0.5d, and Δx_2=0.5d at *d/h*=0.50.

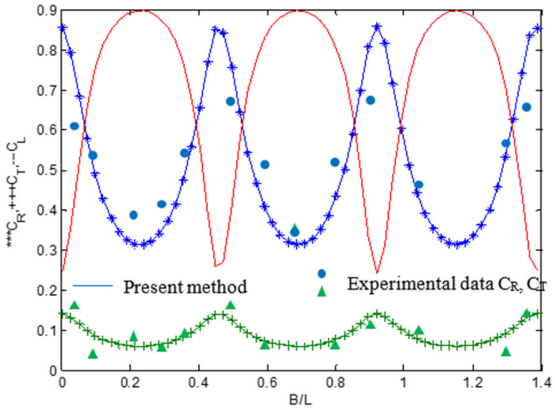

Fig. 9. Comparison between numerical and experimental results: C_R and C_T as a function of *B/L* for k_0h=1.6, G=0.5e^{0i}, Δx_1=0.5d, and Δx_2=0.5d at *d/h*=1.00.

The transmission coefficient C_T exhibits a divergent pattern. It is recognized that the transmission coefficient is maximum for *d/h* = 0.00 and the smallest for *d/h* = 1. For *d/h* = 0.00, it is evident that the transmission and reflection coefficients approximate zero and one, correspondingly. Figures 10 and 11 manifest the dimensionless wave force on the front and rear walls, respectively, as a function of k_0h, with G= 2.00e$^{(9\text{-}1i)}$ and *d/h* = 0.5. As expected, the wave force on the rear wall of the triple-row is less than the wave force on the front wall.

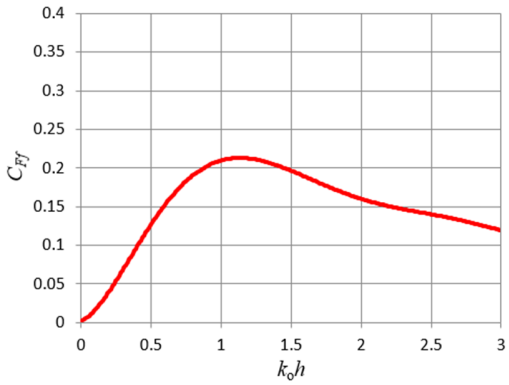

Fig. 10. The dimensionless wave force on the front wall of the triple-row as a function of k_oh, with G = 2.00e$^{(9\text{-}1i)}$ and *d/h* = 0.5.

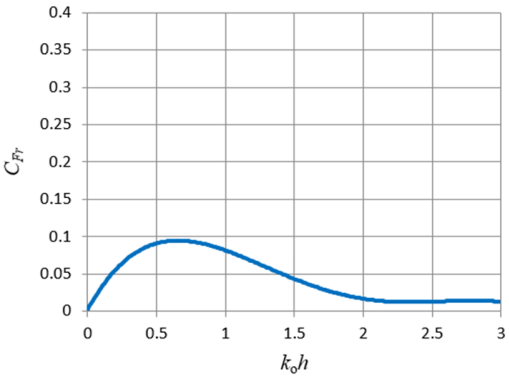

Fig. 11. The dimensionless wave force on the rear wall of the triple-row as a function of k_oh, with G = 2.00e$^{(9\text{-}1i)}$ and *d/h* = 0.5.

The proposed mathematical model was verified by contrasting its results with the experimental and measured results of [5] for a porosity of zero, which causes the model of [5] to become a single impermeable wall. Figure 12 provides a visualization of the proposed model versus the experimental and measured data for the reflection coefficient C_R and the transmission coefficient (C_T) of [5], which are represented as a function of dk_0. The results of the current model roughly coincide with the experimental and measured results of [5].

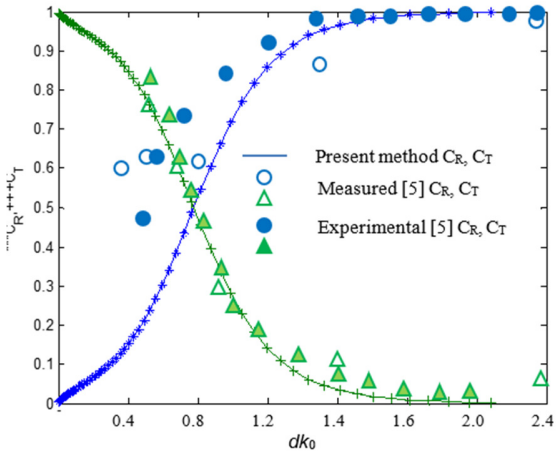

Fig. 12. Comparison between the results of this study with experimental and measured data of [5] for G=∞, k_0h=1.5, and d/h=0.5.

VI. CONCLUSION

This study presents an analytical method for determining the hydrodynamic properties of three rows of vertical permeable wall breakwaters, where the permeable walls were partially submerged in a water channel of constant depth. The method employed in this study is based on a least squares approach and the eigenfunction expansion method. The validity of the proposed methodology was further assessed by comparing its numerical results with measurements from laboratory tests. Good agreement was found between the numerical and experimental results for the C_R, C_T, and C_L coefficients of a partially submerged slotted barrier. This suggests that the recommended mathematical model can accurately reproduce many of the significant features of the experimental results.

The breakwater's reflection coefficient (C_R) and transmission coefficient (C_T), as determined by the numerical method, are primarily dependent on the relative wave chamber width (B/L), the relative draft (d/h), the walls' permeability parameter (G), and the incident wave number (k_0h). For a fixed B/L, an increase in d/h causes an increase in the reflection coefficient (C_R). The transmission coefficient (C_T) exhibits a divergent pattern. It is observed that, in the scenario where the reflection coefficient is maximal for a wall, the transmission coefficient is zero, and the transmission coefficient is maximum for d/h = 0.0 and minimum when d/h = 1. It is clear that when d/h = 0.0, the transmission and reflection coefficients are roughly equal to one and zero, respectively. For fixed B/L, with increasing G, the transmission coefficient increases and the transmission coefficient decreases. The front and middle walls vanish as |G| gets closer to infinity, at which point the C_R and C_T values are constants for the various B/L ratios. When |G| approaches infinity, the C_R and C_T values are both constants for the various values of B/L. When G increases, the calculated transmission coefficients decrease with raising spacing between the first and second rows (Δx_1) for fixed B/L, whereas the calculated reflection coefficients slowly rise with rising Δx_1. For a given B/L, as k_0h increases, the calculated transmission coefficients decrease as Δx_1 increases, whereas the calculated reflection coefficients gradually raise as Δx_1 raises. As the value of k_0h is augmented, the oscillation of the computed transmission and reflection coefficients is augmented. The anticipated hydrodynamic properties for the triple-row walls as a function of k_0h at different row-to-row distances indicate that the C_T exhibits the opposite pattern, increasing with decreasing d/h at fixed k_0h and increasing with increasing k_0h at fixed d/h.

REFERENCES

[1] G. P. Tsinker, Marine Structures Engineering: Specialized Applications. Boston, MA, USA: Springer US, 1995.

[2] G. Elchahal, R. Younes, and P. Lafon, "Optimization of coastal structures: Application on detached breakwaters in ports," *Ocean Engineering*, vol. 63, pp. 35–43, May 2013, https://doi.org/10.1016/j.oceaneng.2013.01.021.

[3] R. Gayen and A. Mondal, "Water wave interaction with two symmetric inclined permeable plates," *Ocean Engineering*, vol. 124, pp. 180–191, Sep. 2016, https://doi.org/10.1016/j.oceaneng.2016.07.045.

[4] A. S. Koraim, M. M. Iskander, and W. R. Elsayed, "Hydrodynamic performance of double rows of piles suspending horizontal c shaped bars," *Coastal Engineering*, vol. 84, pp. 81–96, Feb. 2014, https://doi.org/10.1016/j.coastaleng.2013.11.006.

[5] M. Isaacson, S. Premasiri, and G. Yang, "Wave Interactions with Vertical Slotted Barrier," *Journal of Waterway, Port, Coastal, and Ocean Engineering*, vol. 124, no. 3, pp. 118–126, May 1998, https://doi.org/10.1061/(ASCE)0733-950X(1998)124:3(118).

[6] M. Isaacson, J. Baldwin, S. Premasiri, and G. Yang, "Wave interactions with double slotted barriers," *Applied Ocean Research*, vol. 21, no. 2, pp. 81–91, Apr. 1999, https://doi.org/10.1016/S0141-1187(98)00039-X.

[7] S. Zhu and A. T. Chwang, "Investigations on the reflection behaviour of a slotted seawall," *Coastal Engineering*, vol. 43, no. 2, pp. 93–104, Jun. 2001, https://doi.org/10.1016/S0378-3839(01)00008-4.

[8] K. D. Suh, W. S. Park, and B. S. Park, "Separation of incident and reflected waves in wave–current flumes," *Coastal Engineering*, vol. 43, no. 3, pp. 149–159, Aug. 2001, https://doi.org/10.1016/S0378-3839(01)00011-4.

[9] J. Brossard, A. Jarno-Druaux, F. Marin, and E. H. Tabet-Aoul, "Fixed absorbing semi-immersed breakwater," *Coastal Engineering*, vol. 49, no. 1, pp. 25–41, Aug. 2003, https://doi.org/10.1016/S0378-3839(03)00044-9.

[10] K.-D. Suh, S. Shin, and D. T. Cox, "Hydrodynamic Characteristics of Pile-Supported Vertical Wall Breakwaters," *Journal of Waterway, Port, Coastal, and Ocean Engineering*, vol. 132, no. 2, pp. 83–96, Mar. 2006, https://doi.org/10.1061/(ASCE)0733-950X(2006)132:2(83).

[11] K.-D. Suh, H. Y. Jung, and C. K. Pyun, "Wave reflection and transmission by curtainwall–pile breakwaters using circular piles," *Ocean Engineering*, vol. 34, no. 14, pp. 2100–2106, Oct. 2007, https://doi.org/10.1016/j.oceaneng.2007.02.007.

[12] A. S. Koraim, "Hydrodynamic characteristics of slotted breakwaters under regular waves," *Journal of Marine Science and Technology*, vol. 16, no. 3, pp. 331–342, Sep. 2011, https://doi.org/10.1007/s00773-011-0126-1.

[13] H. Ahmed, A. Schlenkhoff, and M. Oertel, "Stokes second-order wave interaction with vertical slotted wall breakwater," in *Coastal Structures 2011*, World Scientific, 2012, pp. 691–703.

[14] L. Xiao, Y. Kou, L. Tao, and L. Yang, "Comparative study of hydrodynamic performances of breakwaters with double-layered perforated walls attached to ring-shaped very large floating structures," *Ocean Engineering*, vol. 111, pp. 279–291, Jan. 2016, https://doi.org/10.1016/j.oceaneng.2015.11.007.

[15] N. V. Duc, "Improving the Mechanical Performance of Shell Precast Concrete Blocks for Coastal Protection Structures of Hydraulic Works," *Engineering, Technology & Applied Science Research*, vol. 11, no. 1, pp. 6787–6791, Feb. 2021, https://doi.org/10.48084/etasr.4009.

[16] M. O. Alsaydalani, M. A. N. Saif, and M. M. Helal, "Hydrodynamic characteristics of three rows of vertical slotted wall breakwaters," *Journal of Marine Science and Application*, vol. 16, no. 3, pp. 261–275, Sep. 2017, https://doi.org/10.1007/s11804-017-1427-5.

[17] J. Huang and G. Chen, "Experimental modeling of wave load on a pile-supported wharf with pile breakwater," *Ocean Engineering*, vol. 201, Apr. 2020, Art. no. 107149, https://doi.org/10.1016/j.oceaneng.2020.107149.

[18] M. Gandomi *et al.*, "Multi-criteria decision-making optimization model for permeable breakwaters characterization," *Ocean Engineering*, vol. 280, Jul. 2023, Art. no. 114447, https://doi.org/10.1016/j.oceaneng.2023.114447.

[19] "Application of a Fractional Step Algorithm for the Three-Dimensional Shallow Water Equations in a Rotating Spherical Surface," *International Journal of GEOMATE*, vol. 25, no. 107, pp. 123–132, May 2023, https://doi.org/10.21660/2023.107.3830.

[20] T. Eldamaty, A. G. Ahmed, and M. M. Helal, "GIS-Based Multi Criteria Analysis for Solar Power Plant Site Selection Support in Mecca," *Engineering, Technology & Applied Science Research*, vol. 13, no. 3, pp. 10963–10968, Jun. 2023, https://doi.org/10.48084/etasr.5927.

[21] M. Badawi, A. G. Ahmed, T. A. Eldamaty, and M. M. Helal, "The Effect of Polypropylene Fibers on the Fracture Characteristics of Lightweight Aggregate Crumb Rubber Concrete Composites," *Engineering, Technology & Applied Science Research*, vol. 13, no. 3, pp. 10638–10645, Jun. 2023, https://doi.org/10.48084/etasr.5821.

[22] M. Badawi, A. G. Ahmed, T. A. Eldamaty, and M. M. Helal, "Properties of Recycled Concrete utilizing Waste Rubber," *Engineering, Technology & Applied Science Research*, vol. 13, no. 4, pp. 11451–11458, Aug. 2023, https://doi.org/10.48084/etasr.5918.

[23] K. G. Vijay, S. Neelamani, and T. Sahoo, "Wave interaction with multiple slotted barriers inside harbour: Physical and numerical modelling," *Ocean Engineering*, vol. 193, Dec. 2019, Art. no. 106623, https://doi.org/10.1016/j.oceaneng.2019.106623.

[24] E. P. D. Mansard and E. R. Funke, "The Measurement of Incident and Reflected Spectra Using a Least Squares Method," pp. 154–172, Dec. 2015, https://doi.org/10.1061/9780872622647.008.